ACS APPLIED MATERIALS & INTERFACES

Research Article

Cite This: ACS Appl. Mater. Interfaces 2019, 11, 45763−45775

www.acsami.org

Surfactant-Augmented Functional Silica Nanoparticle Based Nanofluid for Enhanced Oil Recovery at High Temperature and Salinity

Yanxia Zhou,[†,‡,§] Xu Wu,[†] Xun Zhong,[∥] Wen Sun,[†] Hui Pu,*[,∥] and Julia Xiaojun Zhao*[,†]

[†]Department of Chemistry, University of North Dakota, Grand Forks, North Dakota 58202, United States

[‡]College of Petroleum Engineering and [§]Key Laboratory of Enhanced Oil Recovery of Education Ministry, Northeast Petroleum University, Daqing, Heilongjiang 163318, China

[∥]Department of Petroleum Engineering, University of North Dakota, Grand Forks, North Dakota 58202, United States

Supporting Information

ABSTRACT: Nanofluids in recent years have shown great potential as a chemical enhanced oil recovery (EOR) technology, thanks to their excellent performance in altering interfacial properties. However, because of the great challenge in preparing stable systems suitable for an elevated temperature and a high salinity environment, expanding the application of nanofluids has been greatly restrained. In this work, a novel nanofluid was prepared by integrating positively charged amino-terminated silica nanoparticles (SiNP-NH_2) with negatively charged anionic surfactant (Soloterra 964) via electrostatic force. The resulted nanofluid could be stored at relatively high salinity (15 wt % NaCl solution) and high temperature (65 °C) for more than 30 days without aggregation. Successful coating of the surfactant on target SiNPs was verified by Fourier transform infrared spectrometry and the surface charge and size distribution. In addition, the potential of the nanofluid in recovering oil was investigated by analyzing the nanofluid/Bakken oil interfacial tension and the variation trend of the oil contact angle when brine was replaced by nanofluids. Experimental results showed that the water−oil interfacial tension of the Bakken crude oil decreased by 99.85% and the contact angle increased by 237.8% compared to the original value of 13.78 mN/m and 43.4°, respectively, indicating strong oil displacement efficiency and obvious wetting transition from oil-wet toward water-wet. Spontaneous imbibition tests conducted on Berea rocks showed that the nanofluid yielded a high oil recovery rate of 46.61%, compared to that of 11.30, 16.58, and 22.89% for brine, pure SiNP-NH_2, and pure surfactant (Soloterra 964), respectively. In addition, when core flooding was applied, a total of 60.88% of the original oil in place could be recovered and an additional oil recovery of 17.23% was achieved in the chemical flooding stage. Moreover, a possible mechanism of the EOR using the nanofluid was proposed. Overall, the developed nanofluid is a promising new material for EOR.

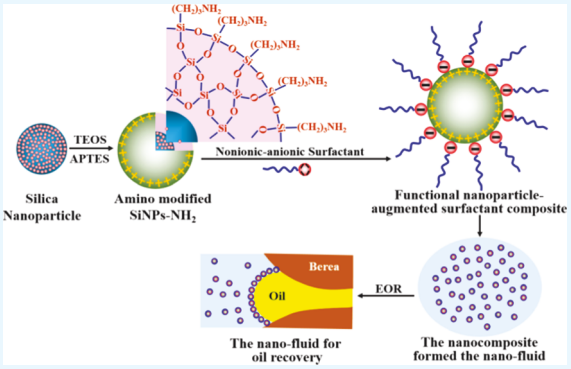

KEYWORDS: *silica nanoparticle, nano-fluid, interfacial tension, oil contact angle, enhanced oil recovery, surfactant*

1. INTRODUCTION

Global demand for oil and natural gas is increasing because of the rapid economic development worldwide.[1−7] In addition to discovering new reservoirs, enhanced oil recovery (EOR) technologies aiming at extracting more oil and gas from the known reservoirs after the primary recovery are of great importance.[8−13] In fact, EOR is more crucial in some known unconventional tight reservoirs because the current horizontal drilling and multistage hydraulic fracturing technologies can only obtain a small portion (5−10%) of the existing oil/gas.[14] What is worse, harsh reservoir conditions including extreme temperature, pressure, and salinity bring additional challenges.[15,16] Therefore, developing suitable EOR fluids that can successfully penetrate into rocks and effectively displace oil being locked in micro- and nanopores becomes an urgent mission.[17,18]

EOR, also known as tertiary recovery, mainly includes three technologies, that is, gas, thermal, and chemical injection. All of them have the capability to reduce residual oil saturation.[19,20] However, at present, most of the world's oilfields are at the middle and late stages of development with approximately two thirds of the oil remaining trapped within the reservoirs even after the previously mentioned conventional EOR agents were added for displacement.[21,22] Novel EOR fluids that could improve oil mobility and/or result in higher swept efficiency are critically needed.[23,24] Recently, nanofluids have attracted great attention in EOR because of several favorable characters of nanomaterials including low cost, low toxicity,[25−27]

Received: September 18, 2019
Accepted: November 15, 2019
Published: November 15, 2019

DOI: 10.1021/acsami.9b16960
ACS Appl. Mater. Interfaces 2019, 11, 45763−45775

ultrasmall size, and high surface-to-volume ratio.[28−31] Generally speaking, contact angle and interfacial tension measurements and displacement tests (spontaneous imbibition test and core flooding test) are necessary to evaluate the performance and EOR potential of a newly developed nanofluid.[20,32,33] Until date, different kinds of metal oxide nanoparticles have been involved in EOR research. For instance, Ogolo et al. investigated the performance of eight NPs (oxides of aluminum, zinc, magnesium, iron, zirconium, nickel, tin, and silicon) on EOR and they discovered that the oil recovery could be increased by 0.8−12.5% with the addition of nanoparticles in distilled water.[34,35] However, different mechanisms have been proposed for nanofluid EOR. Some research groups think that wettability alteration is the main reason.[36−43] For example, Li et al.,[44] Al-Anssari et al.,[45] Roustaei and Bagherzadeh,[46] and Maghzi et al.[47] tested the variation of contact angles with different concentrations of silica nanoparticles (SiNPs). They observed that SiNPs could change the wettability of the formation to more water-wet. While others indicated that the reduction in interfacial tension is also important, Rezvani et al. investigated the interfacial tension between seawater and crude oil reduced from 22.49 to 14.47 mN/m with the increase in nanocomposite concentration.[32] Kazemzadeh et al. showed that the synthesized TiO_2/SiO_2 nanocomposite can reduce the interfacial tension (IFT) between oil and water to 13.2 mN/m compared to that of 39 mN/m for distilled water.[33] Although nanoparticles alone showed excellent performance in altering wettability and enhancing oil recovery, pure particles with a large size naturally tend to aggregate and precipitate when used at high temperatures and high salinities.[48] Thus, particle surface modification is necessary to prepare thermally and kinetically stable nanofluids.[49] Most investigators thought that using surfactants in the nanofluid as a stabilizer and/or synergistic enhancement agents may recover more oil. Zhao et al. showed that surfactant-based silica nano-fluid recovered 16.0% of the original oil in place (OOIP) compared to about 8.0% OOIP for surfactant Triton X-100 solution in a 10 days' spontaneous imbibition experiment.[50] Cheraghian et al. found that the ultimate oil recovery achieved by injecting 2 wt % SiNPs in the sodium dodecyl sulfate surfactant was 13% higher than the ultimate oil recovery by injecting the surfactant alone.[51]

However, most published papers related to nanofluid EOR only focused on nanofluids being used at relatively low temperatures and low salinities. A few efforts have been made to improve the temperature and salinity with a possible result of 50 °C[12] and 7.0 wt % NaCl salinity.[52] In most experiments, the brine prepared with nanofluids is equivalent to NaCl solution. Given the high temperature and high salinity in real oil fields,[45,53] the feasibility of current nano-fluids is extremely limited.

To address this challenge, in this study, we developed a new nanofluid applied in equivalent NaCl salinity by integrating positively charged amino-modified silica nanoparticles (SiNP-NH_2) with the negatively charged anionic surfactant (Soloterra 964) via electrostatic force. The resultant nanofluid showed improved stability at high salinities and high temperatures and also great potential when being used as a promising new material for EOR.

2. EXPERIMENTAL SECTION

2.1. Materials. Analytical grade materials including cyclohexane (anhydrous, 99.5%), 1-hexanol (anhydrous, ≥99.0%), and Triton X-100 were purchased from Sigma-Aldrich. Tetraethyl orthosilicate (TEOS, regent grade, 98.0%), $NH_3{\cdot}H_2O$ (28% NH_3 in H_2O), acetone (≥99.5%), and ethane (≥99.5%) were also purchased from Sigma-Aldrich. 3-Aminopropyltriethoxysilane (APTES) was purchased from Thermo Scientific. Sodium chloride (analytical grade, ≥ 99.5%) was purchased from VWR Chemicals, which was used to prepare a 15.0 wt % NaCl solution with density and dynamic viscosity of 1.04 g/cm^3 and 1.08 mPa·s at 25 °C, respectively. Alcohol polyethylene glycol ether carboxylic sodium (Soloterra 964) surfactant obtained from Sasol was used directly without further purification. Bakken crude oil was used in this experiment with a measured density of 0.82 g/cm^3 and a dynamic viscosity of 2.28 mPa·s at 50 °C and asphaltenes of 0.23%, respectively. Berea outcrop sandstone was purchased from Cleveland Quarries. All the core plugs used were Berea samples with porosity around 18.0% and permeability about 90 × 10^{-3} μm^2.

2.2. Instruments. A transmission electron microscope (TEM, Hitachi 7500) was used to study the morphology of nanoparticles. X-ray diffractometer (XRD, Smartlab-3KW) was used to analyze the phase and the internal molecular information of the Berea core samples. Zeta potential and particle size measurements were carried out based on the dynamic light scattering (DLS) analysis using a Zetasizer (Malvern, Westborough). The infrared spectroscopy analysis was conducted using a Fourier transform infrared spectrometer (FT-IR, Spectrum 400). The porosimeter (TPI-219, Coretest Systems, Inc.) and gas permeameter (TKA-209 Coretest Systems, Inc.) were used for porosity and permeability measurements. The interfacial tension and contact angle were measured using a Pendent Drop Interfacial Tension Cell Model (IFT-10, ramé-hart instrument co.). Both Mixer/Mill (8000M, SPEX Sample Prep) and Shatter Box (8530, SPEX Sample Prep) were used to convert the Berea core sample to some powder for XRD analysis. All core samples were saturated by using Bakken crude oil with a vacuum saturation device (ZYB-II Type, Hai'an Huacheng Scientific Research Instrument Co., Ltd.). The imbibition cell used in the imbibition experiments held the imbibition liquid and Berea core samples. The core flooding system, including an oven (UF260, Wisconsin Oven Distributors, LLC), a core holder (37 181, Vinci Technologies), a pressure sensor (CV-310-HC, Vindum Engineering, Inc.), and a pressure output record (VS15453, ViewSonic), was used to test the oil recovery of oil displacement agents, including the surfactant (Soloterra 964) and SiNP-based nanofluid.

2.3. Synthesis of Amino-Modified Silica Nanoparticles. The SiO_2-NH_2NPs were synthesized using a reverse micro-emulsion method[54] at room temperature. Briefly, a mixture of 7.5 mL of cyclohexane, 1.8 mL of 1-hexanol, and 1.77 mL of TritonX-100 was stirred for 20 min. Then, 480 μL of H_2O was added to form a water-in-oil reverse micro-emulsion. A 100 μL aliquot of TEOS was added dropwise as a precursor for silica formation. After 20 min of stirring, a 100 μL aliquot of $NH_3{\cdot}H_2O$ was added to initiate the polymerization process. This process lasted for 24 h at room temperature to form SiNPs. Afterward, the SiNPs were modified through forming amino groups on the nanoparticle surface by synchronous hydrolysis of 100 μL of TEOS and 20 μL of APTES. Finally, the demulsification of water-in-oil reverse micro-emulsion was performed using acetone, and the SiO_2-NH_2NPs were washed with ethanol and DI water three times using centrifugation, which can obtain about 0.03 g of SiO_2-NH_2NPs in a single patch.

2.4. Preparation of Nanofluid. The nanofluid was prepared by adding different amounts of SiO_2-NH_2NPs (0−0.05 wt %) into the Soloterra 964 surfactant solution (prepared by 15.0 wt % NaCl brine). Herein, the concentration of Soloterra 964 surfactant was maintained at 0.2 wt % which was a little bit higher than its critical micelle concentration (cmc) of 0.19 wt % (Supporting Information Figure S1) because of its absorbance onto the reservoir formation at some degree. To better study the properties of the nanofluid, controls without the surfactant (Si-NPs alone with varying concentrations) were also prepared for contrastive analysis. Both the nanofluid and the control were stirred for 2 h and then ultrasonicated for 2 h to ensure the homogenous distribution of the nanoparticles.

DOI: 10.1021/acsami.9b16960
ACS Appl. Mater. Interfaces 2019, 11, 45763−45775

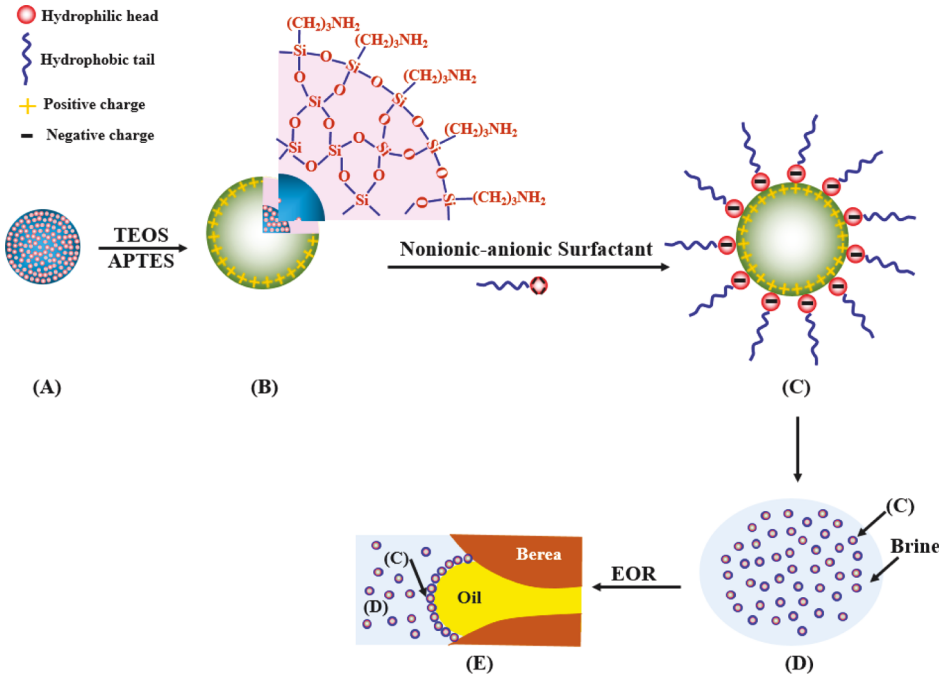

Figure 1. Schematic diagram of the designed nanofluid. (A) A SiNP. (B) Amino-modified SiNPs-NH_2. (C) Surfactant-augmented functional silica nanocomposite. (D) Nanocomposite dissolved in brine formed the nanofluid. (E) Application of the nano-fluid for oil recovery.

2.5. Thermal Stability of the Nanofluid. The thermal ability of the nanofluid was studied based on the variation in the nanoparticle size. Both nanofluid and the corresponding control (10 mL) were placed in an oven at a constant temperature of 65 °C over a 30 day period. The size distributions of the samples were measured every 5 days to monitor if any aggregations occurred at high temperatures.

2.6. Interfacial Tension Measurement. The interfacial tension between Bakken oil and the nanofluid was tested using the inverted pendant drop method at atmospheric pressure and temperature at 65 °C. Both the nanofluid and the control of the nanofluid without the Soloterra 964 surfactant were measured. The measurements were carried out using a system with a stainless steel chamber and two sections being made up of high pressure resistant glass. First, both the nanofluids containing 0.2 wt % Soloterra 964 surfactant and the control with different amounts (0−0.05 wt %) of SiO_2-NH_2NPs were prepared. Then, the fluids to be tested were put inside the chamber and the chamber was equipped with O-rings to seal each connection. Around the chamber, there is some electrical resistance wire to heat the chamber for controlling the temperature of the tested fluids. At the lower-middle part of the chamber, there is an entrance to pump the used fluid. After the target fluid was pumped inside, the entrance was closed. At the bottom of the chamber, there is an entrance to pump the Bakken oil. When the Bakken oil is pumped inside, there will be an inverted pendant oil drop. At right side of the chamber, there is a camera whose center is as high as the chamber, taking the photo of the pendant oil drop after it forming for 1 min at 65 °C and input it to the computer. Then, the shape of an inverted pendant oil drop on a needle in a bulk nanofluid phase was imaged. The interfacial tension was calculated from the image of the drop using a drop shape analysis by a Drop Image software which is a program system for interfacial tension and contact angle measurement by image analysis and is a proprietary product of Finn Knut Hansen that is marketed under an exclusive agreement with ramé-hart instrument company. Averages of three replicates for each sample were obtained for further analysis.

2.7. Oil Contact Angle Measurement. The oil contact angle between the oil and the Berea sample slices in the nanofluid was determined using the sessile drop method. The Berea sample slices were prepared with a diameter of ∼0.5 cm and a length of ∼0.1 cm for testing the contact angle. Prior to the test, these sample slices were aged in Bakken oil at 80 °C and atmospheric pressure for 10 days and later dried in an oven for 1 d at 60 °C. To ensure the rock surface was oil-wet, the contact angle was first measured after the Berea sample slices were completely processed. Also, both the nanofluid and the control of the nanofluid without the Soloterra 964 surfactant were measured. The measurements were carried out using a system mentioned in Section 2.6. First, the nanofluids and the control with different amounts (0−0.05 wt %) of SiO_2-NH_2NPs were prepared. Then, Berea sample slices were stuck onto a handle and inserted from the top of the chamber. From the left side of the chamber, one oil drop onto the Berea sample slice was injected, and then, the left side of the chamber was closed. Next, the fluid to be tested was pumped from the middle-lower part of the chamber, so the oil drop image was captured using the right side camera. The oil droplet was captured on the oil-wet surface of Berea sample slices in a bulk nanofluid phase at 65 °C by using a high-resolution camera on the right side of the chamber. The oil contact angle was measured using a drop image analysis software which is the same as that mentioned above. Averages of three replicates for each sample were obtained for further analysis.

2.8. XRD Analysis of the Berea Core Sample. The XRD analysis of the Berea core sample was determined using the powder <270 mesh. First, the larger Berea chips were placed in the mixer/mill for 5 min to reduce their size to approximately sand size (less than 1 or 2 mm). Then, no more than about 2 g of the coarse grind was transferred to the steel container of the shatter box for 5 min of grinding. After grinding, the powder was sieved through the 270 mesh sieve. At last, the sieved powder was mounted in the sample holder of the XRD to obtain the ultimate quality diffraction data of minerals.

2.9. Spontaneous Imbibition Tests. Prior to the imbibition test, all Berea core samples were cleaned using the Soxhlet extraction method with toluene and methanol to remove organic contaminants and any adsorbed materials. Then, the samples were dried at 80 °C for 48 h to obtain a constant weight. After cooling down to room temperature in a desiccator, the weights of the four core samples were measured using an electronic analytical balance. Then, these cores were vacuumed to remove the gas inside the cores. After 24 h of vacuum cleaning, the porosity and gas permeability were tested using a porosimeter and a gas permeameter, respectively. Then, the sample cores were fully saturated with Bakken crude oil using a core vacuum saturation device. After being saturated, the core samples were aged in

DOI: 10.1021/acsami.9b16960
ACS Appl. Mater. Interfaces 2019, 11, 45763−45775

crude oil for about 10 days at 80 °C at atmospheric pressure to alter the initial wettability. Before the imbibition test, the core samples were measured once more. The OOIP was determined by measuring the weight difference before and after oil saturation. In order to compare the oil recovery of the nanofluid in spontaneous imbibition, three types of imbibition liquids were used as controls, including 15 wt % NaCl brine, 0.2 wt % Soloterra 964 surfactant dissolved in 15 wt % NaCl brine, and the SiO_2-NH_2NPs solution. Their ability to displace oil from core samples was tested at 65 °C. The volume of oil displaced from these cores was measured at the same time.

2.10. Core Flooding Tests. Oil-saturated core, its previous processing steps, and OOIP calculation were coincident with the above Section 2.9. The pore volume (PV) of the core sample was determined by core geometry volume multiplied by porosity. After the process of oil saturation, the Berea core samples were also put in the Bakken oil at 80 °C for 10 days as previously mentioned to make the polar substances such as colloid and asphaltene in crude oil reach adsorption equilibrium on the surface of the rock pores. Before the core flooding started, a rubber sleeve containing the oil-saturated core sample was put into the core holder and then the core holder was placed into the oven. At the same time, the silicone oil between the core holder and rubber sleeve provided a stable confined pressure of 8.0 MPa around the rubber sleeve to stabilize the oil displacement agent to axially displace the core sample at a constant speed. After these steps were completed, the core flooding started. The procedures of core flooding experiments for oil recovery were concluded as follows: 1.5 PV brine flooding; 0.5 PV chemical flooding, finally, 2.0 PV subsequent brine flooding. Their ability to displace oil from the core samples were all tested at a fixed flow of 0.3 mL/min and at a constant temperature of 65 °C. During the chemical flooding, in order to compare the oil recovery of the nanofluid in core flooding, the SiO_2-NH_2NPs and Soloterra 964 surfactant dissolved in simulated brine were used as the controls of the nanofluid. The pressure difference between the displacement fluid inlet and produced liquid outlet was recorded automatically using a pressure sensor by a computer. The volume of oil and water displaced from these cores were manually recorded versus time.

3. RESULTS AND DISCUSSION

3.1. Design of SiNP-Surfactant-Based Nanofluid. The schematic diagram of the designed nanofluid is shown in Figure 1. First, a SiNP was chosen as a carrier (Figure 1A) and then, the SiNP was modified with amino groups on the surface through synchronous hydrolysis of TEOS and APTES to form SiO_2-NH_2NPs (Figure 1B). The modified nanoparticle was linked with the Soloterra 964 surfactant molecules on the surface to form the surfactant-augmented functional silica nanocomposite (Figure 1C). The composites were dissolved in a 15% NaCl solution (Brine) to form the nanofluid (Figure 1D). Finally, the nanofluid was applied to a Berea core sample for oil recovery (Figure 1E).

The SiNPs were chosen as a carrier because of a few major features of the materials. First, the SiNPs are inexpensive and the resource of silica is abundant. Given the large amount of the nanoparticles that would be needed in the oil field, the cost and availability of the nanomaterials would play critical roles regarding the feasibility of the method. The pioneer works of using silica particles in this field have demonstrated the improvement on the wettability of formation to a more water-wet direction[36−39] and have increased oil recovery at a low concentration of SiO_2 NPs.[41−44]

Effective linkage of surfactants to the nanoparticles was challenging in preparing the nanofluid. The methods to conjugate surfactants to NPs could be classified as physical adsorption and chemical binding.[55,56] A few hydrogen binding and mix together methods have been reported under a low salinity and a low temperature.[2,57] Given harsh conditions of real oil fields, high salinity and high temperature in reservoirs, the hydrogen binding methods maybe less practicable for EOR. Thus, the physical adsorption pathway would be considered in this work. Compared with the negatively charged silica NPs used in the literature,[41,42] the positively charged NPs would be more efficient when negatively charged surfactants are employed in preparing the nanofluid. Therefore, in this work, the surface of the SiO_2 NPs was modified with the positively charged amino groups. The negatively charged Soloterra 964 surfactants were then linked to the modified SiNPs via electrostatic force (Figure 1C).

The surfactant not only played the role for pulling out oil from the formation, but also considered as a stabilizer for the surfactant-augmented functional silica nanocomposite. In general, silica NPs were unstable with a tendency to aggregate in the oil field conditions,[45,53] especially under high temperatures and high salinities. The existence of surfactants would effectively reduce the aggregation to maintain nanofluid homogeneous conditions.

Some researchers have applied the surfactant-nanoparticle formulation to get a higher oil recovery.[36−40] Here, the nanofluid was heated at 65 °C to test its stability under this relatively high temperature. Many studies have shown that NPs added into oil displacement agents can alter oil−water interfacial tension[58] and formation wettability,[59−61] which were two important parameters for EOR. Therefore, the interfacial tension and contact angles were investigated using the nanofluid. At last, spontaneous imbibition and displacement experiments were conducted to test its efficiency for EOR after preparing the Berea core samples.

3.2. Characterization of the Modified SiO_2-NH_2NPs and the Surfactant-Augmented Functional Silica Nanocomposite. The developed SiO_2-NH_2NPs were characterized regarding its morphology, structure, size distribution, surface charge, and surface functional groups. The TEM image of the SiO_2-NH_2NPs is shown in Figure 2A. The obtained NPs were amorphous and not crystalline in a spherical shape with a diameter of ca. 40−50 nm. The size and the size distribution were further characterized using a nanoparticle size analyzer as described in the Experimental Section. The obtained hydrodynamic diameter of the nanoparticles and its distribution is shown in Figure 2B with an average size of 50 ± 2.1 nm, which indicated a relatively uniform size and the result was comparable with that from the TEM image.

The surface functional groups on the nanocomposites were confirmed by the FTIR analysis (Figure 2C). First, the synthesized pure SiNPs were dried at 60 °C to obtain the SiNP powder. The FTIR spectrum of the pure SiNPs was recorded as a control (Figure 2C curve (a)). Theoretically, a broad peak at the range of 3200−3400 cm^{-1} on the FTIR spectrum is ascribed to −OH groups. This broad peak was clearly observed in curve (a), indicating the presence of −OH on the pure SiNP surface. A peak at 1095 cm^{-1} was ascribed to the antisymmetric stretching vibration of Si−O−Si.[62−64] Then, the amino-modified SiNPs were detected using the same experimental conditions as shown in the Figure 2C curve (b). Based on the literature, the peak at 3100−3500 cm^{-1} was mainly due to the existence of the $-NH_2$ group.[62−64] Compared to the pure SiNPs, the SiO_2-NH_2NPs has a sharp peak around 3440 cm^{-1}, indicating the presence of $-NH_2$. In addition, two peaks were observed at 1700 and 1630 cm^{-1}, which could be considered as the $-NH_2$ group bending

DOI: 10.1021/acsami.9b16960
ACS Appl. Mater. Interfaces 2019, 11, 45763−45775

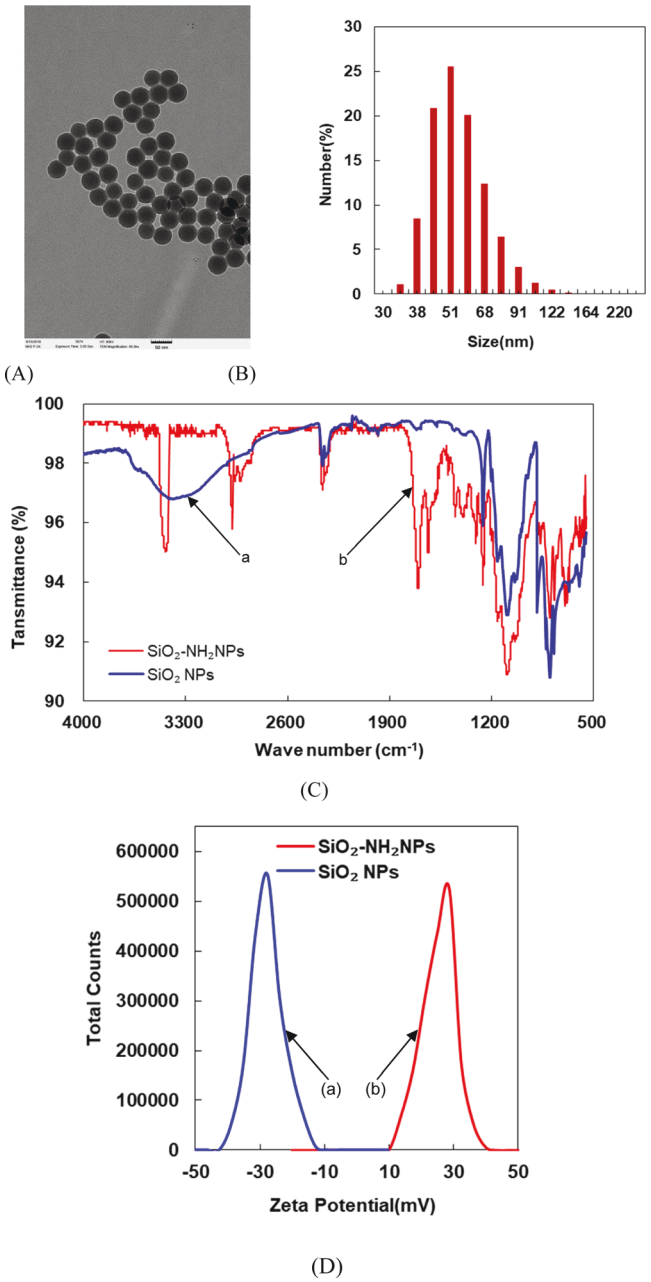

Figure 2. Characterization of modified SiNPs-NH_2. (A) TEM image of the modified SiNPs-NH_2. (B) Particle size distribution in DI water based on the DLS method. (C) FTIR spectra of pure SiNPs (a); and modified SiO_2-NH_2NPs (b). (D) Zeta potential distribution of the pure SiNPs (a) and the modified SiO_2-NH_2NPs (b).

vibration. A similar peak at 1095 cm^{-1} was ascribed to the antisymmetric stretching vibration of Si−O−Si,[62−64] while the peaks at 2960 and 2920 cm^{-1} were ascribed to −CH group. The FTIR results demonstrated the existence of $-NH_2$ groups on the SiO_2 NPs surface.

For further confirmation of the $-NH_2$ modification on the surface, the zeta potential of the modified SiO_2-NH_2NPs was also measured. First, pure SiNPs were measured as a control (Figure 2D curve (a)), which showed a negative zeta potential. In contrast, the curve of the amino-modified SiO_2-NH_2NPs (Figure 2D curve (b)) appeared in the range of positive zeta potential. Given the positively charged amino group, it was evident that the amino groups were modified onto the SiNPs.

The linkage of the Soloterra 964 surfactants to the modified SiNPs was characterized using FTIR spectroscopy. The FTIR spectrum of the Soloterra 964 surfactant was recorded as a control (Figure 3A curve (a)). As shown in Figure 3A, the peak at 1100 cm^{-1} was mainly due to C−O stretching,[62−64] and the peak at 1600−1700 cm^{-1} was mainly ascribed to the vibration of carbonyl groups in carboxylates. These characteristic groups exist in Soloterra 964 surfactant molecules. Then, the obtained surfactant-augmented functional silica nanocomposite was analyzed using the FTIP spectroscopy (Figure 3A curve (b)). Characteristic groups of Soloterra 964 surfactant molecules all appeared in this curve. Additionally, a sharp peak at 3370−3540 cm^{-1} indicated the presence of $-NH_2$ while the peak at 1250−1270 cm^{-1} was the vibration of C−N. Compared to curve (a) and curve (b), it is convincing that the surfactants are linked to the SiNPs.

Furthermore, the zeta potential of the composite was measured with the increment of the Soloterra 964 surfactant concentration at a constant SiO_2-NH_2NPs concentration of 0.05 wt % SiO_2-NH_2NPs in DI water (pH = 7, for the zeta potential under other pH values see Supporting Information Figure S2) at room temperature (Figure 3B). With increasing Soloterra 964 surfactant concentration (wt %) from 0.00, 0.04, 0.08, 0.12, 0.16, to 0.20, the zeta potential initially decreased from a positive charge to a negative charge. When the Soloterra 964 surfactant concertation was higher than 0.12 wt %, the zeta potential reached the plateau of −20 mV. Zeta potential is an important factor of the stability of nanoparticle solution. The higher the absolute value of zeta potential, the more stable nanoparticle solution is.[65] However, this is valid for a pure electric nanoparticle but not for higher or large molecular weight stabilizers, which act mainly by steric stabilization.[66] Therefore, the surfactant-modified nanoparticle had improved stability because of steric stabilization. Meanwhile, the zeta potential of it was a result from the adsorbed surfactant molecules shift the plane of shear to a farther distance from the particle surface, which led to a reduction of the measured zeta potential than original nanoparticles. This meant the zeta potential values were of only 20 mV or much lower for the surfactant-modified nanoparticles can provide sufficient stabilization.

Moreover, the hydrodynamic diameter of the nanocomposites at a constant SiO_2-NH_2NPs concentration of 0.05 and 0.2 wt % Soloterra 964 surfactant was measured. Given the number of negative charges on the surfactant molecules, it could be linked to the positively charged SiO_2-NH_2NPs via electrostatic force. Thus, the surfactant-augmented functional silica nanocomposite would have a larger hydrodynamic diameter. Additionally, the average size and size distributions of the nanocomposite at different conditions was measured. As shown in Figure 3C, in DI water, at room temperature (Figure 3C cure (a)), an average size of 58 ± 1.8 nm was obtained. The size was increased to 65 ± 2.1 nm when the solution salinity increased to 15 wt % of NaCl brine at room temperature (Figure 3C curve (b)). The size change could be associated with the increased salinity of the solution. Additionally, when the temperature increased from room temperature to 65 °C in 15 wt % NaCl brine for 24 h (Figure 3C curve (c)), the size was further increased to 70 ± 3.8 nm. The results indicated that the high temperature and the Brownian motion of the anions and cations might slightly weaken the nanoparticle repulsion though surfactants lined to the modified SiNPs surface.

DOI: 10.1021/acsami.9b16960
ACS Appl. Mater. Interfaces 2019, 11, 45763−45775

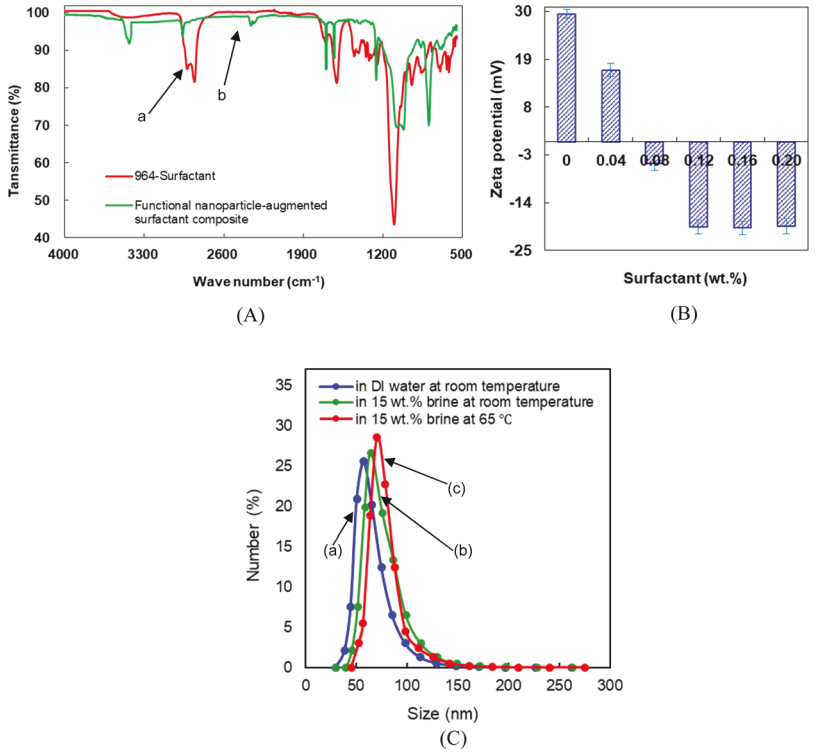

Figure 3. Characterization of the formed surfactant-augmented functional silica nanocomposite. (A) FTIR spectra of the Soloterra 964 surfactant (a); and surfactant-augmented functional silica nanocomposite (b). (B) Zeta potential distribution in DI water (pH = 7) at room temperature. (C) Particle size distribution in DI water at room temperature (a); in 15 wt % NaCl brine at room temperature (b); and in 15 wt % NaCl brine at 65 °C (c).

3.3. Evaluation of Crucial Parameters of the Nano-Fluid for EOR. *3.3.1. Long-Term Thermal Stability of the NanoFluid.* The temperature effect on the thermal stability of the surfactant-augmented functional silica nanocomposite has been briefly studied within a short time period (Figure 3 curve (c)). Considering that the oil recovery is a lengthy process, the nanofluid would have to remain in the high temperature of reservoirs for one month, thus, in order to use the nanofluid in the oil field, the long-term thermal stability of the nanofluid was investigated. A time period of 30 days was chosen for this study. The criterion used for evaluating the thermal stability of the nanofluid was based on their particle size measurement at high temperatures. In general, the reservoir temperature is in the range of 50−100 °C but is more commonly around 60 °C.[67] Here, a temperature of 65 °C was used for the experiment. As described in the Experimental Section, the nanofluid was placed in an oven at 65 °C and the hydrodynamic diameters of the nanoparticles were measured every five days. The size of the particles remained at a constant diameter of 71 nm during the period of 30 days (Figure 4). In contrast, the particle size in the control increased significantly and reached 664.5 ± 3.6 nm after 5 days in the high temperature environment (Figure 4). This indicated the surfactant-augmented functional silica nanocomposite is more stable than the positively charged SiNPs. After a large amount of Soloterra 964 surfactant molecules adsorbed onto the surface of the nanoparticles, the hydrophobic interaction between the hydrophobic groups of the Soloterra 964 surfactant molecules and their steric stability further stabilized the composite. Furthermore, the free surfactant as a stabilizer also contributed to its stability. This is why the composite can stabilize in brine better than positively charged SiNPs. The

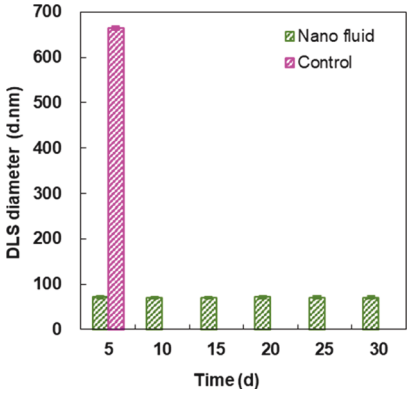

Figure 4. Average particle size after the identical samples were placed at 65 °C for 5, 10, 15, 20, 25, 30 d in 15 wt % NaCl brine.

results showed the enhanced thermal stability of the nanofluid SiO_2-NH_2NPs for a long-term period, which is critical for further EOR applications.

3.3.2. Reduced Interfacial Tension by the NanoFluid. Oil−water interfacial tension is an important parameter for oil recovery. In general, the smaller the interfacial tension between the nanofluid and the oil, the higher the mobility of the oil is. As a result, the EOR rate could be increased. Thus, we measured the oil−water interfacial tension of the nanofluid with the Bakken crude oil as described in the Experimental Section. The control of the nanofluid without the Soloterra 964 surfactant was tested first. As shown in Figure 5, without SiO_2-NH_2NPs and the surfactant, the oil−water interfacial tension between 15 wt % NaCl brine and the Bakken crude oil was 13.78 mN/m. When the different concentration of SiO_2-

DOI: 10.1021/acsami.9b16960
ACS Appl. Mater. Interfaces 2019, 11, 45763−45775

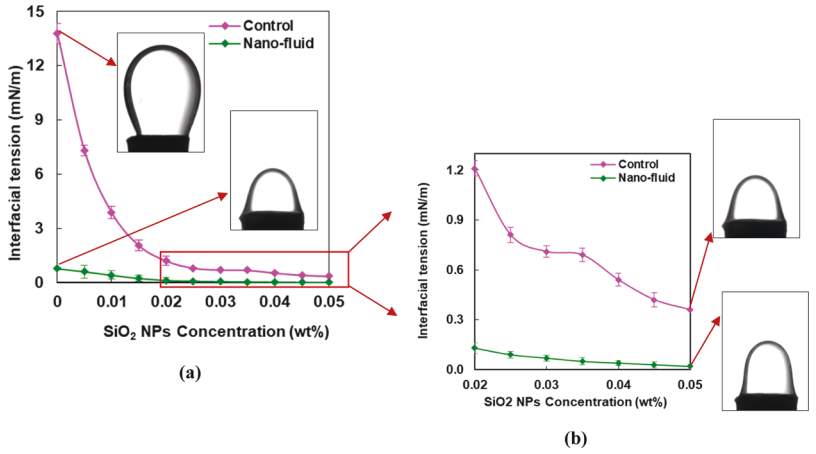

Figure 5. Oil–water interfacial tension of different concentrations of modified SiO_2-NH_2NPs in 15 wt % NaCl at 65 °C: (a) overall data, (b) Zoom image of red area in (a).

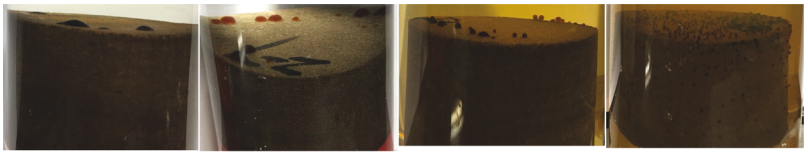

Figure 6. Oil droplets at the surface of Berea samples: (a) in control of 15 wt % NaCl brine; (b) in control of SiNP solution; (c) in control of 0.2 wt % Soloterra 964 surfactant; (d) nanofluid.

NH_2NPs was added to the control, the interfacial tension reduced significantly. As 0.05 wt % NPs was applied, the interfacial tension was reduced to 0.36 mN/m, only 2.6% of the original value. Furthermore, the nanofluid was tested without the SiO_2-NH_2NPs, the oil–water interfacial tension between 0.2 wt % Soloterra 964 surfactant solution and the Bakken crude oil was reduced to 0.78 from 13.78 mN/m, reduced by 94.3%. Although ultralow IFT can be obtained at surfactant cmc, lower interfacial tension would make oil displacement much easier from the surface of the formation, which could improve oil washing efficiency. Therefore, the nanofluid was expected to achieve it. When the SiO_2-NH_2NPs was added, the interfacial tension was further reduced. The reduction percentage was in line with the concentration of the SiO_2-NH_2NPs. As the concentration of SiO_2-NH_2NPs increased to 0.05%, the interfacial value reached as low as 0.02 mN/m, merely 0.15% of the original value. Therefore, the nanofluid significantly reduced the water–oil interfacial tension of the Bakken crude oil by 99.85%.

The lower interfacial tension also reduced the size of the oil droplets on the rock surface, resulting in higher mobility of the oil. The lower the interfacial tension, the smaller the oil droplet is. Photographs of the oil droplets at the surface of the Berea samples in 15 wt % NaCl solution, controls of SiNP solution and Soloterra 964 surfactant, and nanofluid confirmed this hypothesis (Figure 6). The smallest oil droplet in the nanofluid makes the oil flow easily out of the pore of the rock. This is one example that the nanofluid can enhance oil recovery.

A possible theoretical illustration of the effect of interfacial tension reduction on EOR is drawn in the schematic diagram (Figure 7) and discussed in eqs 1 and 2. The decrease of the interfacial tension means the reduction of the adhesion work (the work by pulling the liquid droplets from the solid surface at an interface of 1 cm^2). Therefore, oil mobilization could be

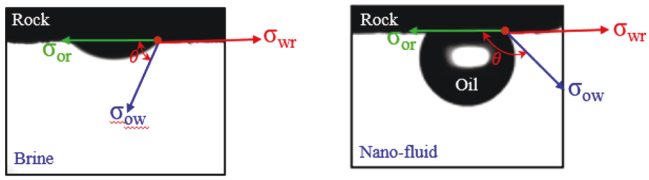

Figure 7. Wetting state of oil on the rock surface: (a) oil-wet state (θ < 90° without nanofluid, in a brine solution), (b) water-wet state ($\theta \geq$ 90° when the nanofluid was used).

improved, and the oil could be easily detached from the formation surface. When the oil droplets reached equilibrium at the rock surface, based on the Young's equation, we obtained

$$\sigma_{wr} = \sigma_{or} + \sigma_{ow} \cos \theta \quad (1)$$

$$W_a = \sigma_{wr} + \sigma_{ow} - \sigma_{or} = \sigma_{ow}(1 + \cos \theta) \quad (2)$$

Where σ_{wr} is the liquid–rock interfacial tension; σ_{or} is the oil–rock interfacial tension; σ_{ow} is the oil–liquid interfacial tension; θ is the contact angle of the oil phase on the rock surface; and W_a is the adhesion work. It is clear that a smaller σ_{ow} leads to a smaller W_a. Figure 5 shows a much lower oil–water interfacial tension when the nanofluid is used. Thus, the adhesion work was reduced significantly to promote the oil displacement.

3.3.3. Measurement of the Contact Angle of Oil with the NanoFluid. Wettability is an important parameter for evaluating the efficiency of an EOR process while the contact angle measurement is a common quantitative method for assessing wettability. Rock wettability can be divided into three categories depending on the value of the oil contact angle, $0 \leq \theta < 75°$ for oil-wet, $75 \leq \theta \leq 105°$ for intermediate wet, and $105 < \theta \leq 180°$ for water-wet.[68] Water-wet condition with a

DOI: 10.1021/acsami.9b16960
ACS Appl. Mater. Interfaces 2019, 11, 45763–45775

large oil contact angle of the oil phase is preferred in an EOR process. The contact angle of oil-saturated core samples moved toward oil-wet because of partial adoption of polar components in crude oil on the sandstone substrate.[69] This was confirmed based on the shape of oil drop contact angle in the presence of air and oil aged core samples (see Supporting Information Figure S3). It was expected that the developed nanofluid could increase the contact angle of the oil phase and thus increase the wettability for an EOR. As described in the Experimental Section, the Berea rock samples were pretreated in the Bakken oil and the contact angles of oil with Berea samples were measured. As a control, the original contact angle of the oil phase in the brine without both SiO_2-NH_2NPs and the Soloterra 964 surfactant was measured to be 43.4° (Figure 8, curve (a)), indicating the oil-wet surface. With the increase

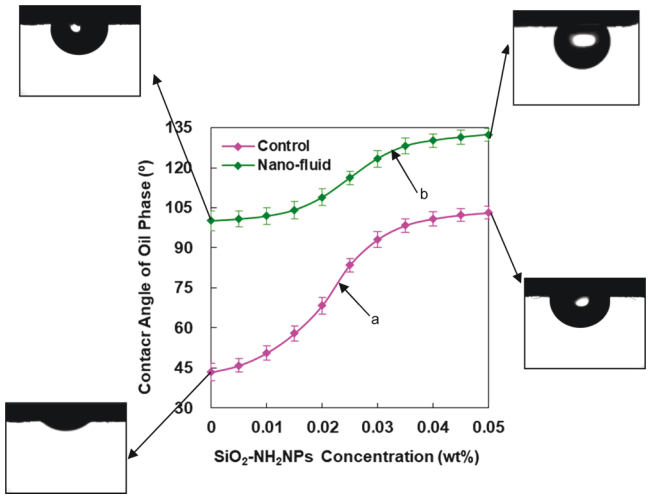

Figure 8. Contact angles of Berea rock samples with the Bakken oil in the nanofluid in different concentrations of SiO_2-NH_2NPs. Curve (a): the control without the Soloterra 964 surfactant. Curve (b): the nanofluid.

of the modified SiO_2-NH_2NPs concentration, the contact angle increased rapidly. When the particle concentration reached 0.035 wt % SiO_2-NH_2NPs, the contact angle increasing extent became insignificant. Eventually, the contact angle reached 103.2° when the concentration of SiO_2-NH_2NPs was 0.05 wt %, increasing by 237.8% compared to the original value. Therefore, in the following spontaneous imbibition test, the concentration of modified SiO_2-NH_2 NPs was chosen to be ≥0.035 wt %.

Afterward, the nanofluid was used for the contact angle test (Figure 8 curve (b)). At the starting point without nanoparticles, the contact angle was 100.1° which was significantly higher than the starting point at curve (a), indicating that the Soloterra 964 surfactant alone could have altered the oil-wet formation to an intermediate wet. When the SiO_2-NH_2NPs was added to form the nanofluid, the contact angle continually increased with a slow pace in the SiO_2-NH_2NPs concentration range of 0−0.025%. Then, the contact angle increased to be larger in the concentration range of 0.025−0.04% of the SiNPs-NH_2. Finally, the oil contact angle slowly reached a plateau of 130.2° after 0.04% of the nanoparticles was used, indicating the water-wet formation. Compared with the control, the contact angle of nanofluid alerted the oil wettability from oil-wet to water-wet. In the following experiments, the concentration of modified SiO_2-NH_2NPs was 0.04 wt % in the nanofluid.

The wettability largely determines oil displacement efficiency. Berea (mainly composed of silicates) originally is the water-wet solid. The oil film on the surface of sandstones should be easily displaced by water. However, because of long-term exposure to crude oil, the active components (colloid and asphaltene) of crude oil adsorbed on the surface of rocks and the wettability of the Berea core samples were changed to oil-wet.[32,33] It was difficult to replace the oil film attached to the Berea surface by water. For SiO_2-NH_2NPs solutions, acidic components of adsorbed colloid and asphaltene on the rock surface are negatively charged and the SiO_2-NH_2NPs is positively charged. With increasing amount of SiO_2-NH_2NPs, more and more SiO_2-NH_2NPs adsorbed on the surface of the rock, which made the rock surface more water wettability because of the SiO_2-NH_2NPs hydrophilic nature, as shown in Figure 8 curve a. For the nanofluid, when the rock sample was in contact, with increasing the amount of SiO_2-NH_2NPs, more and more hydrophobic groups (from the Soloterra 964 surfactant) adsorbed the organic active components on the rock surface, and more and more hydrophilic groups (from the SiO_2 NPs) turned the rock surface to water-wet, as shown in Figure 8 curve b. According to eqs 1 and 2, when σ_{ow} is constant, $W_a < \sigma_{ow}$ on the water-wet rock surface. With the increase of water wettability, the contact angle on the formation surface increased and W_a decreased. The nanofluid provided a higher contact angle and further decreased W_a, which improved oil mobilization.

3.4. EOR Potential. *3.4.1. Berea Core Sample Analysis.* Prior to EOR investigation, the Berea rock samples were analyzed regarding their porosity, permeability, and oil saturation. The results for the imbibition test and core flooding are shown in Table 1. The composition of the Berea rock was further measured using XRD analysis. The XRD results showed that quartz and orthoclase were the main

Table 1. Physical Properties of Berea Core Samples

sample		oil displacing agent	length, cm	diameter, cm	porosity, %	permeability, 10^{-3} μm^2	oil saturation, %
for imbibition test	B1	control of 15 wt % NaCl brine	3.183	2.549	18.56	90.82	94.18
	B2	control of SiNP solution	3.256	2.551	18.68	89.27	93.77
	B3	control of 0.2 wt % Soloterra 964 surfactant	3.112	2.538	18.01	88.62	92.94
	B4	nano-fluid	3.093	2.543	18.25	91.39	94.51
for core flooding experiment	S1	control of SiNP solution	5.256	3.812	18.94	90.96	94.05
	S2	control of 0.2 wt % Soloterra 964 surfactant	5.112	3.808	19.02	91.11	93.87
	S3	nano-fluid	5.093	3.813	18.96	91.08	93.92

DOI: 10.1021/acsami.9b16960
ACS Appl. Mater. Interfaces 2019, 11, 45763−45775

minerals in the Berea core sample with the content of 70.98 and 13.7 wt %, respectively, confirming Berea is sandstone. Additionally, the rock contains 6.4% of illite, 4.4% of aluminum epidote, 2.32% ankerite, and 2.2% kaolinite.

3.4.2. Spontaneous Imbibition Test. The reduced interfacial tension and the enhanced stability and wettability of nanofluid for Bakken oil provided a strong foundation for applications of the nanofluid to EOR. Thereafter, the EOR efficiency of the nanofluid was investigated using the spontaneous imbibition tests. Three different fluids, including 15 wt % NaCl brine, SiNP solution, and 0.2 wt % Soloterra 964 surfactant, were prepared as controls for the nanofluid. As described in Experimental Section, a series of spontaneous imbibition tests were carried out (Figure 9) at 65 °C and

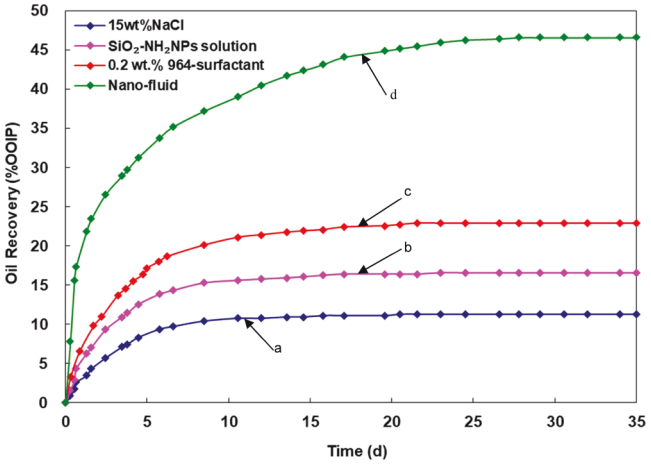

Figure 9. Oil recoveries of spontaneous imbibition experiments in different imbibition liquids at 65 °C in 35 d. Curve (a): the control of 15 wt % NaCl brine. Curve (b): the control of SiNP solution. Curve (c): the control of 0.2 wt % Soloterra 964 surfactant. Curve (d): the nanofluid.

atmospheric pressure. For the three controls, imbibition mainly occurred in the first 3 days and the recovery reached a plateau after 10 days. The final oil recoveries of 15 wt % NaCl brine (Figure 9 cure (a)), SiO_2-NH_2NPs (Figure 9 cure (b)), and 0.2 wt % Soloterra 964 surfactant (Figure 9 cure (c)) were 11.30, 16.58, and 22.89% of OOIP, respectively. The SiO_2-NH_2NPs recovered additional 5.28% OOIP oil than that of 15 wt % NaCl brine. In contrast, the imbibition of the nanofluid mainly occurred in the first 12 days. Then, the recovery continuously increased with a slow pace until 20 days when the oil recovery reached the plateau. At this moment, the oil recovery of the nanofluid reached 46.61% OOIP. This result indicated that the developed nanofluid could be a promising and efficient fluid for EOR.

The above imbibition experiment showed that the oil recovery of nanofluid was higher than the sum of the surfactant and the nanoparticle solution alone. Thus, a synergistic effect among the surfactant and nanoparticles was formed in the nanofluid. Compared to the SiO_2-NH_2NPs, the nanofluid enhanced the dispensability and stability for EOR. Compared to the surfactant, the nanofluid obtained a lower interfacial intension and stronger water wettability. Overall, the synergistic effect significantly enhanced oil recovery.

3.4.3. Core Flooding Test. The EOR efficiency of the nanofluid was investigated using the core flooding tests. The SiNP solution and Soloterra 964 surfactant of 0.2 wt % were prepared as controls for the nanofluid. As described in Experimental Section (experimental flow scheme see Supporting Information Figure S4), the core flooding tests were carried out. The oil recovery of different displacement stages is shown in Table 2. At the first brine flooding stage, the oil recoveries of

Table 2. Oil Recovery of the Core Flooding Test

		oil recovery(%)			
core sample	type of chemical flooding	brine flooding	chemical flooding	subsequent brine flooding	total recovery
S1	control of SiNP solution	38.36	5.32	1.53	45.21
S2	control of 0.2 wt % Soloterra 964 surfactant	38.29	8.61	2.53	49.43
S3	nano-fluid	38.51	17.23	5.14	60.88

the three oil displacement agents were very close. The small difference between them was due to the slight difference in the core and operational error. Therefore, their subsequent experimental data is comparable. Compared with controls of the SiNP and surfactant flooding which enhanced oil recovery by 5.32 and 8.61%, respectively, the oil recovery using the nanofluid was enhanced by 17.23%. This indicated that the oil recovery of the nanofluid flooding was 3.30% higher than the sum of the SiNPs and surfactant flooding in the chemical flooding stage. This also proved that there was a synergistic effect among the surfactant and nanoparticles in the nanofluid. Moreover, in subsequent brine flooding, compared with sum recovery of the SiNPs and surfactant flooding, nanofluid flooding EOR by 1.08% because of its more water wettability. This result indicates that the developed nanofluid had higher oil displacement efficiency and could be a promising and efficient fluid for EOR.

In addition, the dynamic characteristic curve of Berea core flooding is shown in Figure 10. In brine flooding, the oil recovery, pressure difference, and water fraction with the nanofluid flooding was almost coincidental as those of the controls of the SiNPs and surfactant flooding. While in 0.5 PV chemical flooding stage, the oil recovery (Figure 10A cure (c)) and pressure difference (Figure 10B cure (c)) of the nanofluid were both much higher than those of controls (Figure 10A cure (a) and (b), Figure 10 cure (a) and (b)) which indicated that the nanofluid has a much higher capability to extract oil than SiNPs and the surfactant. Additionally, the water fraction of nanofluid (Figure 10C cure (c)) can be greater reduced than those of controls (Figure 10C cure (a) and (b)) which indicates that the nanofluid can displace the remaining oil area that the controls do not reach. More crude oil was produced which reduced water content. In subsequent brine flooding, although the oil recovery and pressure difference trends were slowing down for all the flooding, the nanofluid flooding was still a little bit higher than controls because of nanocomposites retained in the formation. Although the water fraction of the production fluid of the three displacement modes was increasing rapidly, the nanofluid flooding has a little slower upward trend than the two controls' flooding.

Through analyzing, on the one hand, under low interfacial tension, the oil droplets are easily deformed and easy to flow in the core porous medium. On the other hand, higher oil phase wettability reduces the adhesion of oil droplets on the rock surface. Therefore, more and more oil droplets are displaced

DOI: 10.1021/acsami.9b16960
ACS Appl. Mater. Interfaces 2019, 11, 45763−45775

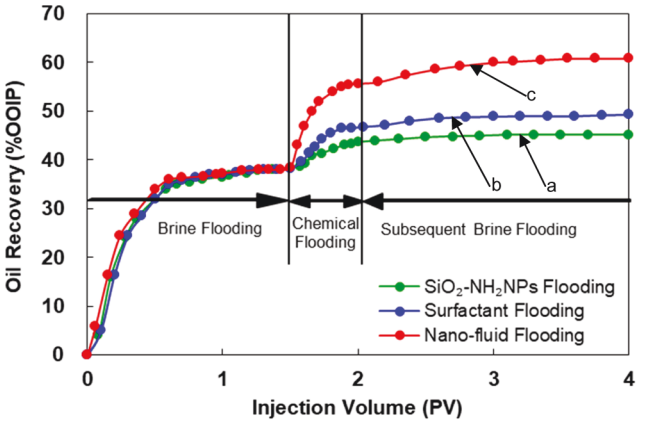

(A)

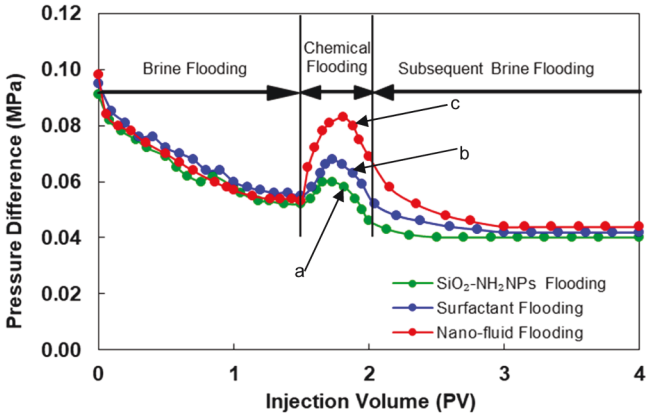

(B)

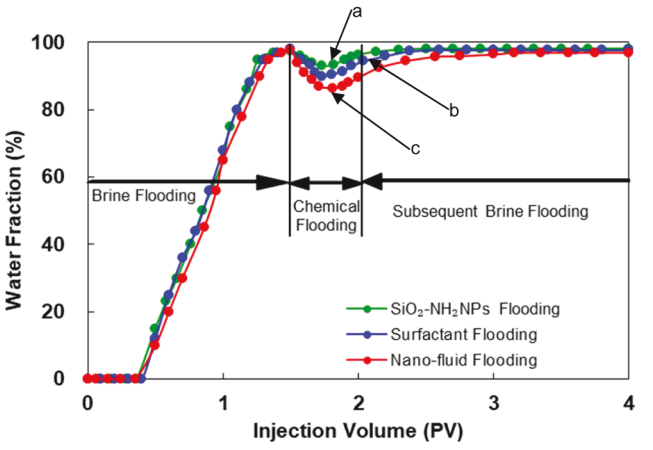

(C)

Figure 10. Dynamic characteristic curve in Berea core flooding. (A) Oil recovery of control of SiNP flooding (a); control of Soloterra 964 surfactant flooding (b); and nanofluid flooding (c). (B) Pressure difference of control of SiNP flooding (a); control of Soloterra 964 surfactant flooding (b); and nanofluid flooding (c). (C) Water fraction of produced liquid of control of SiNP flooding (a); control of Soloterra 964 surfactant flooding (b); and nanofluid flooding (c).

from the surface of the core sample, which improves the oil displacement efficiency of the nanofluid and increases the oil recovery rate. At the same time, the extracted oil droplets collide with each other when moving forward so that the oil beads gather and gradually form an oil belt, and the oil belt merges with more oil beads, resulting in the displacement resistance increasing, causing the displacement pressure to rise, which improved the swept volume. That caused the residual oil to be further displaced to the outlet of the produced liquid, thereby reducing the water fraction of the production liquid.

The above core flooding experiment showed that the oil recovery of nanofluid was higher than the SiNPs and Soloterra 964 surfactant solution. Compared to the SiNPs and surfactant, the nanofluid obtained a lower interfacial intension and stronger water wettability and enhanced the swept volume. Overall, oil droplets that gather into oil bands significantly affect the EOR.

3.5. Potential Mechanism of the NanoFluid for Oil Recovery. In addition to the interfacial intention reduction and the increase of the contact angle and the swept volume discussed above, for oil-wet reservoirs, the possible mechanism of the nanofluid for EOR might be related to reducing capillary resistance in reservoirs. The capillary force is the resistance of water displacement and is descried in eq 3 below.[70]

$$P_c = \frac{2\sigma \cos\theta}{r} \tag{3}$$

where P_c—capillary force; σ—oil−water interfacial tension; r—capillary radius; θ—contact angle of oil on rock surface. (1) When $\theta < 90°$ (oil-wet formation), the greater θ, the smaller capillary resistance; (2) when $\theta = 90°$ (intermediate wet reservoir), $P_c = 0$, the capillary resistance disappears; (3) when $\theta > 90°$ (water wet formation), the wettability changes from the oil-wet into the water-wet. Then, the capillary force changes from migration resistance to a self-suction driving force. According to eq 3, the capillary force of a thin capillary is greater than that of a thick capillary. Thus, imbibition agents could easily enter the thin capillary. Therefore, when $\theta > 90°$, with the wetting angle increasing, the self-priming power increased, and the nanofluid could enter the capillary with a smaller radius, which was the original inaccessible capillary. This could enlarge the sweep coefficient and improve the oil recovery.

4. CONCLUSIONS

In conclusion, after Soloterra 964 surfactant molecules adsorbed onto the surface of the nanoparticles, the hydrophobic interaction between the hydrophobic groups of the surfactant molecules and their steric stabilization improved the nanofluid stability. Furthermore, the free surfactant as a stabilizer also contributed to its stability. The developed nanofluid effectively lowered interfacial tension and improved water wettability and the swept volume. When it was applied to oil recovery, it yielded the oil recovery rate of 46.61% OOIP in spontaneous imbibition, which was 7.13% OOIP higher than the combined oil recovery of SiNPs and Soloterra 964 surfactant solution alone and yielded the total oil recovery rate of 60.88% OOIP in core flooding, which was 3.30% OOIP higher than the combined ones in the chemical flooding stage. A possible mechanism of reducing the capillary resistance of oil-wet reservoirs for EOR was proposed for the nanofluid. Nanoparticle-based nanofluid can promote wettability alteration and interfacial tension reduction and the swept volume, which are beneficial for EOR. Furthermore, nanoparticles have a very large area-to-volume ratio result in their surfaces and can be modified by conjugation or grafting different kinds of molecules. This can make it possible to develop a nanofluid that has specific physical properties according to different

DOI: 10.1021/acsami.9b16960
ACS Appl. Mater. Interfaces 2019, 11, 45763−45775

formations. This is important for the industrial application of nanofluid in oilfields. Although both the temperature and salinity in real oil fields are much higher than of what we have discussed here, the results demonstrated the potential of using the nanofluid as an environment-friendly oil displacement for EOR and pave the way for its applications in oil fields.

■ ASSOCIATED CONTENT

Supporting Information

The Supporting Information is available free of charge at https://pubs.acs.org/doi/10.1021/acsami.9b16960.

cmc of the 964-surfactant; zeta potential of surfactant-augmented functional silica nanocomposite at different pH values; contact angle among the oil/air/oil saturated Berea core sample; and the experimental flow scheme of core flooding (PDF)

■ AUTHOR INFORMATION

Corresponding Authors

*E-mail: hui.pu@und.edu (H.P.).
*E-mail: julia.zhao@und.edu (J.X.Z.).

ORCID

Yanxia Zhou: 0000-0003-1561-8922
Xu Wu: 0000-0003-1336-9571
Hui Pu: 0000-0003-3074-3705
Julia Xiaojun Zhao: 0000-0002-9603-666X

Notes

The authors declare no competing financial interest.

■ ACKNOWLEDGMENTS

This work was supported by the North Dakota Industrial Commission Oil and Gas Research Program (contract no.: G-041-081), the NSF grant CHE 1709160, UND Vice President for Research & Economic Development Postdoctoral Funding Program. The authors acknowledge the use of the Edward C. Carlson Imaging and Image Analysis Core Facility which is supported in part by NIH grant 1P30GM103329. We are very grateful to Sarah Reagen of the department of chemistry at the University of North Dakota for editing this paper.

■ REFERENCES

(1) Li, Y.; Dai, C.; Zhou, H.; Wang, X.; Lv, W.; Wu, Y.; Zhao, M. A Novel Nanofluid Based on Fluorescent Carbon Nanoparticles for Enhanced Oil Recovery. *Ind. Eng. Chem. Res.* **2017**, *56*, 12464−12470.

(2) Nourafkan, E.; Hu, Z.; Wen, D. Nanoparticle-Enabled Delivery of Surfactants in Porous Media. *J. Colloid Interface Sci.* **2018**, *519*, 44−57.

(3) Luo, P.; Luo, W.; Li, S. Effectiveness of Miscible and Immiscible Gas Flooding in Recovering Tight Oil from Bakken Reservoirs in Saskatchewan, Canada. *Fuel* **2017**, *208*, 626−636.

(4) Yang, P.; Guo, H.; Yang, D. Determination of Residual Oil Distribution during Waterflooding in Tight Oil Formations with NMR Relaxometry Measurements. *Energy Fuels* **2013**, *27*, 5750−5756.

(5) Ahmadi, M. A.; Shadizadeh, S. R. Adsorption of Novel Nonionic Surfactant and Particles Mixture in Carbonates: Enhanced Oil Recovery Implication. *Energy Fuels* **2012**, *26*, 4655−4663.

(6) Amirian, E.; Dejam, M.; Chen, Z. Performance Forecasting for Polymer Flooding in Heavy Oil Reservoirs. *Fuel* **2018**, *216*, 83−100.

(7) Unsal, E.; ten Berge, A. B. G. M.; Wever, D. A. Z. Low Salinity Polymer Flooding: Lower Polymer Retention and Improved Injectivity. *J. Pet. Sci. Eng.* **2018**, *163*, 671−682.

(8) Cao, W.; Xie, K.; Lu, X.; Liu, Y.; Zhang, Y. Effect of Profile-control Oil-displacement Agent on Increasing Oil Recovery and Its Mechanism. *Fuel* **2019**, *237*, 1151−1160.

(9) Xie, K.; Lu, X.; Li, Q.; Jiang, W.; Yu, Q. Analysis of Reservoir Applicability of Hydrophobically Associating Polymer. *SPE J.* **2016**, *21*, 001−009.

(10) Xie, K.; Lu, X.; Pan, H.; Han, D.; Hu, G.; Zhang, J.; Zhang, B.; Cao, B. Analysis of Dynamic Imbibition Effect of Surfactant in Microcracks of Reservoir at High Temperature and Low Permeability. *Proceedings of SPE Production & Operations*, 2018.

(11) Bai, Y.; Wang, Z.; Shang, X.; Dong, C.; Zhao, X.; Liu, P. Experimental Evaluation of a Surfactant/compound Organic Alkalis Flooding System for Enhanced Oil Recovery. *Energy Fuels* **2017**, *31*, 5860−5869.

(12) Chen, C.; Wang, S.; Kadhum, M. J.; Harwell, J. H.; Shiau, B.-J. Using Carbonaceous Nanoparticles as Surfactant Carrier in Enhanced Oil Recovery: A laboratory study. *Fuel* **2018**, *222*, 561−568.

(13) Guo, C.; Xu, J.; Wei, M.; Jiang, R. Experimental Study and Numerical Simulation of Hydraulic Fracturing Tight Sandstone Reservoirs. *Fuel* **2015**, *159*, 334−344.

(14) Ma, J.; Wang, X.; Gao, R.; Zeng, F.; Huang, C.; Tontiwachwuthikul, P.; Liang, Z. Enhanced Light Oil Recovery from Tight Formations through CO_2 Huff 'n' Puff Processes. *Fuel* **2015**, *154*, 35−44.

(15) Puerto, M.; Hirasaki, G. J.; Miller, C. A.; Barnes, J. R. Surfactant Systems for EOR in High-Temperature, High-Salinity Environments. *SPE J.* **2012**, *17*, 11−19.

(16) Al-Sahhaf, T.; Elkamel, A.; Suttar Ahmed, A.; Khan, A. R. The Influence of Temperature, Pressure, Salinity, and Surfactant Concentration on the Interfacial Tension of the N-Octane-Water System. *Chem. Eng. Commun.* **2005**, *192*, 667−684.

(17) Słowakiewicz, M.; Perri, E.; Tucker, M. E. Micro-and Nanopores in Tight Zechstein 2 Carbonate Facies form the Southern Permian Basin, NW Europe. *J. Pet. Geol.* **2016**, *39*, 149−168.

(18) Baek, S.; Akkutlu, I. Y. Recovery Mechanisms for Nano-Confined Oil in Source Rocks using Lean Gas Injection. *SPE Western Regional Meeting*; San Jose, California, USA, April 23−26, 2019.

(19) Terry, R. E. Enhanced Oil Recovery. *Encyclopedia of Physical Science and Technology*; Academic Press, 2001; Vol. *18*, pp 503−518.

(20) Sagala, F.; Montoya, T.; Hethnawi, A.; Vitale, G.; Nassar, N. N. Nanopyroxene-Based Nanofluids for Enhanced Oil Recovery in Sandstone Cores at Reservoir Temperature. *Energy Fuels* **2019**, *33*, 877−890.

(21) Muggeridge, A.; Cockin, A.; Webb, K.; Frampton, H.; Collins, I.; Moulds, T.; Salino, P. Recovery Rates, Enhanced Oil Recovery and Technological Limits. *Philos. Trans. R. Soc., A* **2014**, *372*, 20120320.

(22) Kathel, P.; Mohanty, K. K. Wettability Alteration in a Tight Oil Reservoir. *Energy Fuels* **2013**, *27*, 6460−6468.

(23) Kazemzadeh, Y.; Shojaei, S.; Riazi, M.; Sharifi, M. Review on Application of Nanoparticles for EOR Purposes: A Critical Review of the Opportunities and Challenges. *Chin. J. Chem. Eng.* **2019**, *27*, 237−246.

(24) Kazemzadeh, Y.; Sharifi, M.; Riazi, M. Mutual Effect of Fe_3O_4/Chitosan Nanocomposite and Different Ions in Water for Stability of Water-in-oil (w/o) Emulsions at Low-high Salinities. *Energy Fuels* **2018**, *32*, 12101−12117.

(25) Finkenauer, L. R.; Lu, Q.; Hakem, I. F.; Majidi, C.; Bockstaller, M. R. Analysis of the Efficiency of Surfactant-mediated Stabilization Reactions of EGaIn Nanodroplets. *Langmuir* **2017**, *33*, 9703−9710.

(26) Nwidee, L. N.; Lebedev, M.; Barifcani, A.; Sarmadivaleh, M.; Iglauer, S. Wettability Alteration of Oil-wet Limestone Using Surfactant-nanoparticle Formulation. *J. Colloid Interface Sci.* **2017**, *504*, 334−345.

(27) Moghadam, T. F.; Azizian, S. Effect of ZnO Nanoparticle and Hexadecyltrimethylammonium Bromide on the Dynamic and Equilibrium Oil−Water Interfacial Tension. *J. Phys. Chem. B* **2014**, *118*, 1527−1534.

DOI: 10.1021/acsami.9b16960
ACS Appl. Mater. Interfaces 2019, 11, 45763−45775

(28) Lugo, D. M.; Oberdisse, J.; Lapp, A.; Findenegg, G. H. Effect of Nanoparticle Size on the Morphology of Adsorbed Surfactant Layers. *J. Phys. Chem. B* **2010**, *114*, 4183−4191.
(29) Ray, D.; Kumar, S.; Aswal, V. K.; Kohlbrecher, J. Tuning Nanoparticle−Micelle Interactions and Resultant Phase Behavior. *Langmuir* **2018**, *34*, 259−267.
(30) Pilapil, B. K.; Jahandideh, H.; Bryant, S. L.; Trifkovic, M. Stabilization of Oil-in-Water Emulsions with Noninterfacially Adsorbed Particles. *Langmuir* **2016**, *32*, 7109−7116.
(31) Li, R.; Chai, Y.; Jiang, Y.; Ashby, P. D.; Toor, A.; Russell, T. P. Carboxylated Fullerene at the Oil/Water Interface. *ACS Appl. Mater. Interfaces* **2017**, *9*, 34389−34395.
(32) Rezvani, H.; Riazi, M.; Tabaei, M.; Kazemzadeh, Y.; Sharifi, M. Experimental Investigation of Interfacial Properties in the EOR Mechanisms by the Novel Synthesized Fe_3O_4@Chitosan Nanocomposites. *Colloids Surf., A* **2018**, *544*, 15−27.
(33) Kazemzadeh, Y.; Sharifi, M.; Riazi, M.; Rezvani, H.; Tabaei, M. Potential Effects of Metal Oxide/SiO_2 Nanocomposites in EOR Processes at Different Pressures. *Colloids Surf., A* **2018**, *559*, 372−384.
(34) Ogolo, N. A.; Olafuyi, O. A.; Onyekonwu, M. O. Enhanced Oil Recovery using Nanoparticles. *Proceedings of the SPE Saudi Arabia Section Technical Symposium and Exhibition*: Al-Khobar, Saudi Arabia, April 8−11, 2012.
(35) Bayat, A. E.; Junin, R.; Samsuri, A.; Piroozian, A.; Hokmabadi, M. Impact of Metal Oxide Nanoparticles on Enhanced Oil Recovery from Limestone Media at Several Temperatures. *Energy Fuels* **2014**, *28*, 6255−6266.
(36) Hendraningrat, L.; Li, S.; Torsater, O. Effect of Some Parameters Influencing Enhanced Oil Recovery Process Using Silica Nanoparticles: An Experimental Investigation. *Proceedings of the SPE Reservoir Characterization and Simulation Conference and Exhibition*: Abu Dhabi, UAE, September 16−18, 2013.
(37) Ehtesabi, H.; Ahadian, M. M.; Taghikhani, V.; Ghazanfari, M. H. Enhanced Heavy Oil Recovery in Sandstone Cores Using TiO_2. *Energy Fuels* **2014**, *28*, 423−430.
(38) El-Diasty, A. I. The Potential of Nanoparticles to Improve Oil Recovery in Bahariya Formation, Egypt: An Experimental Study. *Proceedings of the SPE Asia Pacific Enhanced Oil Recovery Conference*: Kuala Lumpur, Malaysia, August 11−13, 2015.
(39) Ragab, A. M.; Hannora, A. E. A Comparative Investigation of Nano Particle Effects for Improved Oil Recovery−Experimental Work. *Proceedings of the SPE Kuwait Oil and Gas Show and Conference*: Mishref, Kuwait, October 11−14, 2015.
(40) Hendraningrat, L.; Li, S.; Torsæter, O. A Coreflood Investigation of Nanofluid Enhanced Oil Recovery. *J. Pet. Sci. Eng.* **2013**, *111*, 128−138.
(41) Hu, Z.; Zhao, J.; Gao, H.; Nourafkan, E.; Wen, D. Transport and Deposition of Carbon Nanoparticles in Saturated Porous Media. *Energies* **2017**, *10*, 1151−1167.
(42) Baalousha, M.; Sikder, M.; Prasad, A.; Lead, J.; Merrifield, R.; Chandler, G. T. The Concentration- Dependent Behaviour of Nanoparticles. *Environ. Chem.* **2016**, *13*, 1−3.
(43) Zallaghi, M.; Kharrat, R.; Hashemi, A. Improving the Microscopic Sweep Efficiency of Water Flooding Using Silica Nanoparticles. *J. Pet. Explor. Prod. Technol.* **2018**, *8*, 259−269.
(44) Li, S.; Hendraningrat, L.; Torsaeter, O. Improved Oil Recovery by Hydrophilic Silica Nanoparticles Suspension: 2 Phase Flow Experimental Studies. *Proceedings of the IPTC 2013: International Petroleum Technology Conference*; European Association of Geoscientists & Engineers: Beijing, China, March 26−28, 2013.
(45) Al-Anssari, S.; Barifcani, A.; Wang, S.; Maxim, L.; Iglauer, S. Wettability Alteration of Oil-wet Carbonate by Silica Nanofluid. *J. Colloid Interface Sci.* **2016**, *461*, 435−442.
(46) Roustaei, A.; Bagherzadeh, H. Experimental Investigation of SiO_2 Nanoparticles on Enhanced Oil Recovery of Carbonate Reservoirs. *J. Pet. Explor. Prod. Technol.* **2015**, *5*, 27−33.
(47) Maghzi, A.; Mohammadi, S.; Ghazanfari, M. H.; Kharrat, R.; Masihi, M. Monitoring Wettability Alteration by Silica Nanoparticles during Water Flooding to Heavy Oils in Five-Spot Systems: A Pore-Level Investigation. *Exp. Therm. Fluid Sci.* **2012**, *40*, 168−176.
(48) Kim, I.; Taghavy, A.; DiCarlo, D.; Huh, C. Aggregation of Silica Nanoparticles and Its Impact on Particle Mobility under High-salinity Conditions. *J. Pet. Sci. Eng.* **2015**, *133*, 376−383.
(49) Choudhary, R.; Khurana, D.; Kumar, A.; Subudhi, S. Stability Analysis of Al_2O_3/Water Nanofluids. *J. Exp. Nanosci.* **2017**, *12*, 140−151.
(50) Zhao, M.; Lv, W.; Li, Y.; Dai, C.; Wang, X.; Zhou, H.; Zou, C.; Gao, M.; Zhang, Y.; Wu, Y. Study on the Synergy between Silica Nanoparticles and Surfactants for Enhanced Oil Recovery during Spontaneous Imbibition. *J. Mol. Liq.* **2018**, *261*, 373−378.
(51) Cheraghian, G.; Kiani, S.; Nassar, N. N.; Alexander, S.; Barron, A. R. Silica Nanoparticle Enhancement in the Efficiency of Surfactant Flooding of Heavy Oil in a Glass Micromodel. *Ind. Eng. Chem. Res.* **2017**, *56*, 8528−8534.
(52) Salem, R. A. M., Hannora, A. E. An Experimental Investigation of Silica Nano Particles for Enhanced Oil Recovery Applications. *Proceeding of SPE North Africa Technical Conference and Exhibition Held in Cairo, Egypt*, September 14−16, 2015.
(53) Bagwe, R. P.; Hilliard, L. R.; Tan, W. Surface Modification of Silica Nanoparticles to Reduce Aggregation and Nonspecific Binding. *Langmuir* **2006**, *22*, 4357−4362.
(54) He, X.; Nie, H.; Wang, K.; Tan, W.; Wu, X.; Zhang, P. In Vivo Study of Biodistribution and Urinary Excretion of Surface-Modified Silica Nanoparticles. *Anal. Chem.* **2008**, *80*, 9597−9603.
(55) Müller, J.; Bauer, K. N.; Prozeller, D.; Simon, J.; Mailänder, V.; Wurm, F. R.; Winzen, S.; Landfester, K. Coating Nanoparticles with Tunable Surfactants Facilitates Control over the Protein Corona. *Biomaterials* **2017**, *115*, 1−8.
(56) Hotze, E. M.; Phenrat, T.; Lowry, G. V. Nanoparticle Aggregation: Challenges to Understanding Transport and Reactivity in the Environment. *J. Environ. Qual.* **2010**, *39*, 1909−1924.
(57) Khalafi, E.; Hashemi, A.; Zallaghi, M.; Kharrat, R. An Experimental Investigation of Nanoparticles Assisted Surfactant Flooding for Improving Oil Recovery in a Micromodel System. *J. Pet. Environ. Biotechnol.* **2018**, *9*, 1−6.
(58) Monfared, A. D.; Ghazanfari, M. H.; Jamialahmadi, M.; Helalizadeh, A. Potential Application of Silica Nanoparticles for Wettability Alteration of Oil-wet Calcite: A Mechanistic Study. *Energy Fuels* **2016**, *30*, 3947−3961.
(59) Lim, S.; Horiuchi, H.; Nikolov, A. D.; Wasan, D. Nanofluids Alter the Surface Wettability of Solids. *Langmuir* **2015**, *31*, 5827−5835.
(60) Al-Khafaji, A.; Neville, A.; Wilson, M.; Wen, D. Effect of Low Salinity on the Oil Desorption Efficiency from Calcite and Silica Surfaces. *Energy Fuels* **2017**, *31*, 11892−11901.
(61) Hu, Z.; Haruna, M.; Gao, H.; Nourafkan, E.; Wen, D. Rheological Properties of Partially Hydrolyzed Polyacrylamide Seeded by Nanoparticles. *Ind. Eng. Chem. Res.* **2017**, *56*, 3456−3463.
(62) Kumar, S.; Rai, S. B. Spectroscopic Studies of L-Arginine Molecule. *Indian J. Pure Appl. Phys.* **2010**, *48*, 251−255.
(63) Coates, J. Interpretation of Infrared Spectra, A Practical Approach. *Encyclopedia of Analytical Chemistry;* Wiley, 2000; pp 10815−10837.
(64) Germar, F. V.; Barth, A.; Mäntele, W. Structural Changes of the Sarcoplasmic Reticulum Ca^{2+}-ATPase upon Nucleotide Binding Studied by Fourier Transform Infrared Spectroscopy. *Biophys. J.* **2000**, *78*, 1531−1540.
(65) Jacobs, C.; Kayser, O.; Müller, R. H. Nanosuspensions as a New Approach for the Formulation for the Poorly Soluble Drug Tarazepide. *Int. J. Pharm.* **2000**, *196*, 161−164.
(66) Quaglia, F.; Ostacolo, L.; Mazzaglia, A.; Villari, V.; Zaccaria, D.; Sciortino, M. T. The Intracellular Effects of Nonionic Amphiphilic Cyclodextrin Nanoparticles in the Delivery of Anticancer Drugs. *Biomaterials* **2009**, *30*, 374−382.
(67) Zhou, Z.; Cui, X.; Zhang, W. The Relationship between Formation Temperature and Permeability in a Heavy Oil Reservoir. *Pet. Sci. Technol.* **2016**, *34*, 31−36.

DOI: 10.1021/acsami.9b16960
ACS Appl. Mater. Interfaces 2019, 11, 45763−45775

(68) DiCarlo, D. A.; Akshay, S.; Akshay, S.; Blunt, M. J. Three-Phase Relative Permeability of Water-Wet, Oil-Wet, and Mixed-Wet Sandpacks. *SPE J.* **2000**, *5*, 82−91.
(69) Zhong, X.; Pu, H.; Zhou, Y.; Zhao, J. X. Comparative Study on the Static Adsorption Behavior of Zwitterionic Surfactants on Minerals in Middle Bakken Formation. *Energy Fuels* **2019**, *33*, 1007−1015.
(70) Yang, S. *Reservoir Physics*; Petroleum Industry Press: Beijing, 2011; pp 3350−3360.

DOI: 10.1021/acsami.9b16960
ACS Appl. Mater. Interfaces 2019, 11, 45763−45775